TOPICAL REVIEW

Phase behaviors of ionic liquids attributed to the dual ionic and organic nature

To cite this article: Chenyu Tang and Yanting Wang 2022 *Commun. Theor. Phys.* **74** 097601

Commun. Theor. Phys. **74** (2022) 097601 (15pp) https://doi.org/10.1088/1572-9494/ac7e2a

Topical Review

Phase behaviors of ionic liquids attributed to the dual ionic and organic nature

Chenyu Tang (唐晨宇)[1,2] and Yanting Wang (王延颋)[1,2]

[1] CAS Key Laboratory of Theoretical Physics, Institute of Theoretical Physics, Chinese Academy of Sciences, Beijing 100190, China
[2] School of Physical Sciences, University of Chinese Academy of Sciences, Beijing 100049, China

E-mail: wangyt@itp.ac.cn

Received 31 May 2022, revised 30 June 2022
Accepted for publication 1 July 2022
Published 29 August 2022

Abstract

Ionic liquids (ILs), also known as room-temperature molten salts, are solely composed of ions with melting points usually below 100 °C. Because of their low volatility and vast amounts of species, ILs can serve as 'green solvents' and 'designer solvents' to meet the requirements of various applications by fine-tuning their molecular structures. A good understanding of the phase behaviors of ILs is certainly fundamentally important in terms of their wide applications. This review intends to summarize the major conclusions so far drawn on phase behaviors of ILs by computational, theoretical, and experimental studies, illustrating the intrinsic relationship between their dual ionic and organic nature and the crystalline phases, nanoscale segregation liquid phase, IL crystal phases, as well as phase behaviors of their mixture with small organic molecules.

Keywords: ionic liquids, phase behaviors, nanoscale segregation liquid, ionic liquid crystal

(Some figures may appear in colour only in the online journal)

1. Introduction

Ionic liquids (ILs) are a type of salts with low melting points, often below 100 °C, meaning that they tend to remain in the liquid phase at room temperature and are believed to exhibit some unique features because of the strong electrostatic interactions among ions. Typical aprotic ILs are normally composed of small anions and bulky cations with a long alkyl side-chain and a charged head group, as shown in figure 1, which demonstrates the chemical structure of 1-butyl-3-methylimidazolium chloride, a typical imidazolium-based IL. Possessing both ionic and organic features, they are believed to have advantageous properties of both organic liquids and inorganic salts, such as good solvation ability and tunability, low melting temperature, good conductivity, wide electrochemical window, thermal and electrochemical stabilities, non-volatility, and non-flammability [1–3]. They are thus regarded as 'green' and 'engineer' solvents that can be utilized under many industrial circumstances [4–10].

Understanding the fundamental properties of ILs, particularly their phase behaviors, is essential to their applications. To investigate their phase behaviors, many computational and experimental methods have been employed to investigate phase behaviors of ILs. Molecular dynamics (MD) simulation has become an important means of studying structures and dynamics of ILs [11–14] where different modelling methods that employ various software packages including GROMACS, NAMD, LAMMPS, etc [15–17] have been developed. All-atom force fields are commonly used in addressing IL-related problems by means of MD simulation [18–20], and the applicability of some commonly used all-atom force fields, including the Amber force field [21], OPLS force field [22], CHARMM force field [23], etc, to IL systems, has been verified and the models have been constantly improved to be better applied to ILs [14, 24–34]. By considering the polarizable effect at the atomic level, a polarizable model has also been developed to better quantify the microscopic structures and dynamics of ILs [35–37]. Another modelling strategy is

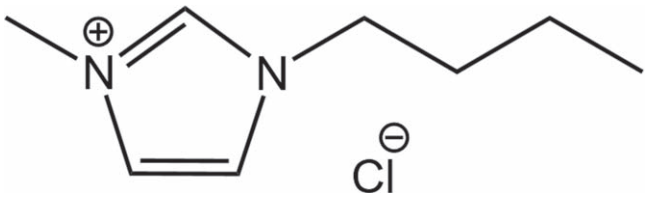

Figure 1. Chemical structure of 1-butyl-3-methylimidazolium chloride.

to apply a coarse-grained (CG) model in MD simulation, which reduces the cost of computation and renders researchers with longer simulated times than all-atom models. One of the CG methods that is used in the context of ILs is the Multiscale Corse-Graining (MS-CG) method [38–40], which matches the instantaneous forces applied to atoms in the all-atom MD simulation to determine the optimal empirical CG forces between CG sites (atomic groups). By contrast, the effective force coarse-graining (EF-CG) method directly calculates the effective averaged force between each pair of CG sites (atomic groups) to gain better transferability [41, 42]. Other MD methods applicable to study ILs include *ab initio* MD [25, 43–45], MD with a polarized force field [46–53], and MD with other CG models [54–59]. Apart from MD simulations, Monte Carlo (MC) simulations [60–62], electronic correlation method [63–66], and density functional theory (DFT) calculations [67–71] are also applied to studying ILs, coming up with many favorable results.

As typical complex liquids, ILs usually have abundant and distinctive phase behaviors beyond the description of simple liquid theories. Some unique phases, including the nanoscale segregation liquid (NSL) phase [72–76], ionic liquid crystal (ILC) phases [77–82], the 'partially arrested' glassy phase [83], and the metastable crystal phase [84], were revealed by MD simulation and verified by experiment. Much attention has been aroused since the detailed knowledge of these phases can shed light on the understanding of not only ILs but also other amphiphilic complex liquids. It also provides guidance for industrial utilizations of ILs as novel solvents. In this review, we majorly focus on summarizing the phase behaviors of aprotic ILs with alkyl cationic side chains whose number of atomic groups is even. We will show that these behaviors tend to be affected highly by temperature, length of the cationic alkyl side-chains, charge distribution, and nature of cations and anions, indicating that these unique phase behaviors of ILs result from their dual ionic and organic nature [85]. By reviewing these phase behaviors and the associated affecting factors and mechanisms, we aim to inspire further investigations in this direction and invite more researchers to delve into this field to develop a thorough understanding of ILs in the future.

2. Dual ionic and organic nature of ILs

One of the most significant features of ILs that broadens their industrial usage is that ILs inherit both the ionic nature of inorganic salts and the organic nature of organic solvents. They have the advantages of non-flammability, non-volatility, good stability, and conductivity compared to organic solvents, and low melting temperature compared to traditional inorganic salts. By varying cations and anions, millions of available ILs can be produced with various physical and chemical properties [6], which is highly beneficial to meeting certain requirements for designated applications. However, since selecting an appropriate combination of cation and anion via experiment is usually tedious or even unfeasible, it is critical to have a good knowledge of the dual ionic and organic nature of ILs to help achieve computer-aided systematic design of ILs. It has been well acknowledged that the competition between electrostatic and van der Waals (VDW) interactions is the key factor characterizing the ionic and organic nature [86, 87], so analyzing these interactions in ILs by means of MD simulations with suitable force fields should be informative.

In a recent work, Shi and Wang [85] performed a series of all-atom MD simulations for four representative ILs (1-butyl-3-methylimidazolium nitrate ([BMIM][NO_3]), 1-butyl-3-methylimidazolium tetrafluoroborate ([BMIM][BF_4]), 1-butyl-3-methylimidazolium hexafluorophosphate ([BMIM][PF_6]), and 1-butyl-3-methylimidazolium bis(trifluoromethylsulfonyl)imide ([BMIM][Tf_2N])), and compared them with three molecular systems with different charge distributions: a typical molten inorganic salt (molten sodium chloride, NaCl), a strongly polar liquid (dimethyl sulfoxide, DMSO), and a weakly polar liquid (toluene). The dual ionic and organic nature of ILs can be depicted from the viewpoint of the cage energy landscape (CEL) by the obtained forces, vibrational force constants, intrinsic electric fields, cohesive energies, and cage energies.

By introducing the concept of ion cage [88–96], which indicates how each ion is surrounded by several counter-ions in the first coordination shell, along with its counterpart of molecular cage [97–101] for molecular liquids, it is possible to depict the structures and dynamics of various types of liquids since the cage volume corresponds to density and the cage stability reflects dynamics. From cage structure, it is then possible to determine CEL by calculating the ensemble-averaged local energy landscape as a function of the dislocation of the central ion from the cage center. The curvature, slope, and depth of CEL can be determined as the force constant k, force F, and activation energy E_a, which is the average energy of a particle required to climb over the energy barrier and escape the cage calculated by using the harmonic approximation (figure 2(a)).

Shi and Wang [85] employed the first moment of the vibrational density of state (VDOS) to qualitatively describe the average characteristic frequency of intermolecular vibrational modes, defined as [102]

$$\langle\omega\rangle = \int_0^{\omega_c} \omega I(\omega)\mathrm{d}\omega / \int_0^{\omega_c} I(\omega)\mathrm{d}\omega, \tag{1}$$

where ω is the frequency and $I(\omega)$ the VDOS. The total, VDW, and electrostatic forces, respectively, are compared in all the investigated liquids, and the liquid-phase cage energy U_{cage} is defined as the average potential energy between an ion

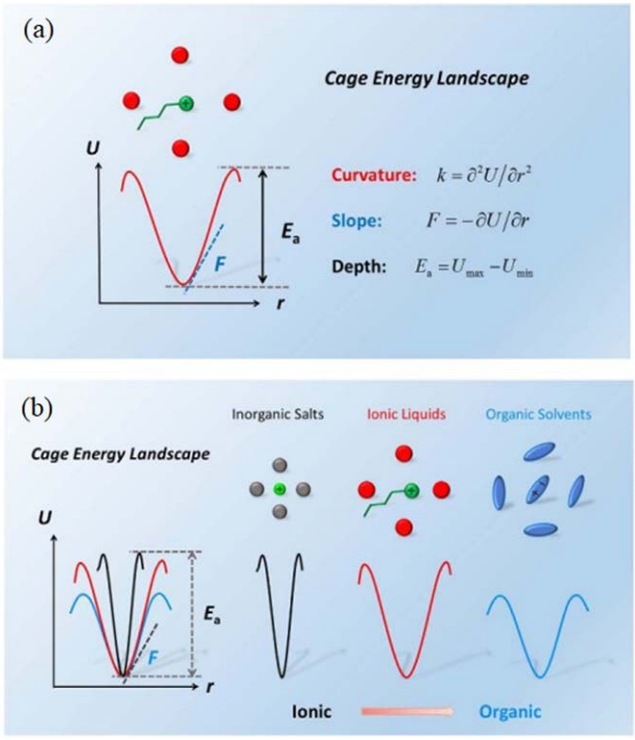

Figure 2. (a) Cage energy landscape characterized by curvature, slope, and depth, corresponding to force constant, force, and activation energy experienced by molecules, respectively. (b) Schematic illustration of cage structures and cage energy landscape in inorganic salts, ionic liquids, and organic solvents. The cage energy landscape of inorganic salts is deep and steep, whereas that of ionic liquids is still deep but much more gently. Organic solvents and ionic liquids have a similar slope and curvature near the minimum of the cage energy landscape, but the depths for the organic solvents are much lower. Reprinted with permission from [85].

and a counter-ion in its ion cage to characterize the local ion–ion interaction in the liquid.

From these approaches, a conclusion has been drawn that similar molecular size, geometry, and component lead to comparable VDW forces in organic ions and organic molecules. They also weaken the electrostatic interactions in ILs because of charge delocalization and charge transfer. The cage energy of ILs induced by electrostatic interactions is drastically different from organic liquids. These findings indicate that the VDW interactions, which dominate the intermolecular forces and vibrational force constants, characterize the organic nature of RTILs, resulting in a similar geometry near the minimum of the CEL to organic liquids; whilst the cage energy, or the depth of the CEL, can characterize their ionic nature (figure 2(b)). Such a mechanism explains the similar and dissimilar characteristics between ILs and organic liquids, and it clarifies the blurry dual ionic and molecular nature of ILs whereas the corresponding microscopic mechanism provides new insights into their phase behaviors.

3. Nanoscale segregation liquid (NSL) phase

A unique phase behavior in ILs that can be explained by the dual ionic and organic nature of ILs is the nanoscale segregation liquid (NSL) phase of ILs, which is different from either the simple liquid phase or the liquid crystal (LC) phase. The structure was first discovered by MD simulation and later verified by experiment [73, 75, 103, 104]. The discovery of the NSL phase may possibly boost new industrial applications of ILs, and the microscopic mechanism of NSL shall aid the engineering of ILs [75]. The significance of this discovery is enhanced by the fact that the NSL exists in most IL systems with an amphiphilic cation, independent of a specific choice of the anion.

In a series of MS-CG MD simulations on $[C_nMIm][NO_3]$ with $n = 4$–12, Wang *et al* [73–75] observed a tail-aggregation phenomenon and later referred to it as the nanoscale segregation liquid (NSL) phase, as shown in figure 3. It has been found that, in a certain temperature range, while the whole liquid is macroscopically homogeneous, the tail groups of the cationic alkyl side chains form nanoscale nonpolar tail domains microscopically segregated with the continuous polar network formed by charged anions and cationic head groups. The existence of the NSL phase was later confirmed by experiments [103, 105, 106] using optical heterodyne-detected Raman-induced Kerr effect spectroscopy (OHDRIKES), neutron diffraction, x-ray diffraction, electrospray ionization mass spectrometry (ESI-MS), and NMR measurements, as well as simulation works [107–109].

To quantify the degree of tail aggregation in the NSL phase, the Gaussian-like heterogeneity order parameter (HOP) is defined as [75]

$$h = \frac{1}{N}\sum_{i,j=1}^{N} \exp\left(-\frac{r_{ij}^2}{2\sigma^2}\right) \tag{2}$$

to quantify the spatial heterogeneity for identical sites, where r_{ij} is the distance between sites i and j, and $\sigma = L/N^{1/3}$ with L being the side length of the cubic simulation box and N being the total number of identical sites.

Both the radial distribution functions (RDFs) and HOPs of the simulated systems show that, compared with ILs with short alkyl side chains, which is basically in the simple liquid phase, the tail groups distribute quite heterogeneously in ILs with an intermediate alkyl side chain length. The charged domain, constituted by anions and cationic head groups, is dominated by the electrostatic interactions, whereas the neutral cationic tail groups form a nonpolar tail domain with the VDW interactions among tail groups. It has also been discovered that such aggregation behavior is temperature-sensitive, which can be understood through analyzing the tail domain diffusion in ILs [75]. Investigating the behavior of tail domains with increasing temperature has also revealed that the transition of ILs from NSL to simple liquid is characterized by the collective behavior of tail groups. Nevertheless, such a collective behavior is passively induced by the steric repulsion from the continuous polar network, as concluded by a further study on ILs with an external electric field applied that the repulsion from the polar part is the major cause of the aggregation of the nonpolar tail groups [76].

4. ILC phases

While ILs with an intermediate cationic alkyl side-chain length can form the unique NSL phase, it has been revealed

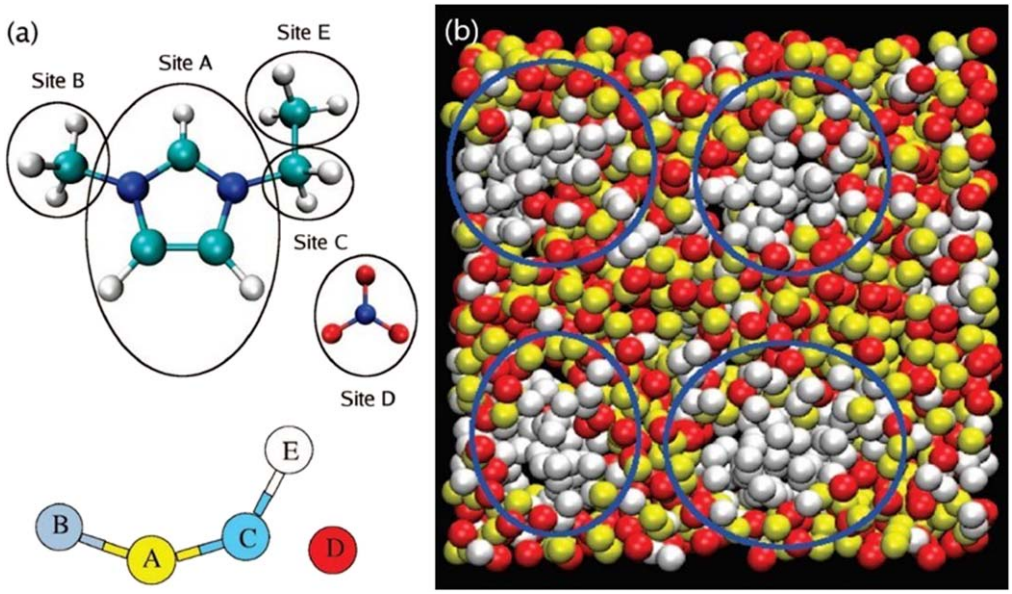

Figure 3. (a) Molecular structure and coarse-graining scheme for the simulated IL. (b) Snapshot illustrating the NSL phase. The white spheres represent the cationic terminal groups, the gold spheres represent the cationic head groups, and the red spheres represent the anions. The ellipses in blue indicate the approximate positions of the nonpolar tail domains. Reprinted with permission from [104]. Copyright 2007 American Chemical Society.

by experiment that ILs with longer alkyl chains can easily form ILC phases, most of which are smectic [79, 80, 82, 110–115]. It is therefore critical to unveil the mechanism for ILs to transform from NSL to ILC phases when the length of alkyl side chains increases. To study this phase transition, Ji *et al* [81] and Li *et al* [116] adopted the EF-CG model for ILs [42] to perform MD simulations on $[C_n\text{MIm}][NO_3]$ with $n =$ 6–22 [81] and 12–24 [116], respectively. Both simulations indicate that the phase transition from NSL to ILC exists when the side-chain length is increased.

Ji *et al* [81] have simulated 512 ion pairs with an isotropic barostat and cubic simulation box. The HOP values reveal that the IL systems go through a structural transition when the side-chain length increases beyond 14, and the HOP of tail groups decreases drastically from C_{14} to C_{16} (figure 4(a)). It not only coincides with previous experimental studies [82] but also is verified through RDFs of the investigated systems. The orientation correlation function (OCF) for side chains has also been introduced, which is the ensemble-averaged correlation between the orientations of two side chains as a function of the distance between the center-of-masses (COMs) of cations:

$$C(r) = \langle [3(\hat{u}(\vec{r}_i) \cdot \hat{u}(\vec{r}_j))^2 - 1] \cdot \delta(\vec{r} - \vec{r}_i + \vec{r}_j)/2 \rangle, \quad (3)$$

where $\hat{u}(\vec{r}_i)$ is the unit vector pointing from the head to the tail of the ith cation.

As shown in figure 4(b), the maximum value of OCF increases with the side-chain length from 6 to 14, and stays close to 1 from 16 to 22, indicating that the side chains of neighboring cations change their relative spatial feature from aggregated to parallel-aligned. It can also be observed that, with increasing distance, the OCF values for C_6 to C_{14} gradually decrease to zero and those for C_{16} to C_{22} gradually decrease to a finite value. This provides further evidence that the transformation is a phase transition from the NSL phase to the ILC-like phase since, in the NSL phase, side chains do not have long-range correlations, whereas they have a long-range order in the ILC-like phase. It has been suggested that the increment of the VDW interactions might be the major cause for such a transition.

Li *et al*'s work [116] further investigated this phase transition and interpreted it from the perspective of the percolation phase transition. Larger systems (4096 ion pairs) have been simulated with an anisotropic barostat allowing the simulation box size in three dimensions to change independently and an isotension-isothermal ensemble allowing the simulation box to change its shape. In the configurations equilibrated by simulating annealing procedures, two side chains are considered 'connected' when their COM distance is less than 0.72 nm and at the same time the twist angle between them is less than 30°. A set of 'connected' side chains is then defined as a cluster. In IL systems with an intermediate side-chain length, such as C_{12}, the side chains have weak tendencies to form clusters (figure 5(a)). With increasing side-chain length, in the C_{16} system, more and larger clusters formed locally because of the stronger tendency of parallel alignment of side chains, but the orientations of the clusters are still random (figure 5(b)). For C_{22}, side chains are in parallel globally and the largest cluster is comparable to the size of the simulated box, and the second-largest cluster is comparatively very small (figure 5(c)), implying the occurrence of a percolation phase transition [117, 118]. By analysing the size difference between the largest and second-largest clusters (figure 5(d)), it has been determined that the phase transition happens at C_{18} where both the average cluster size and the correlation length reach

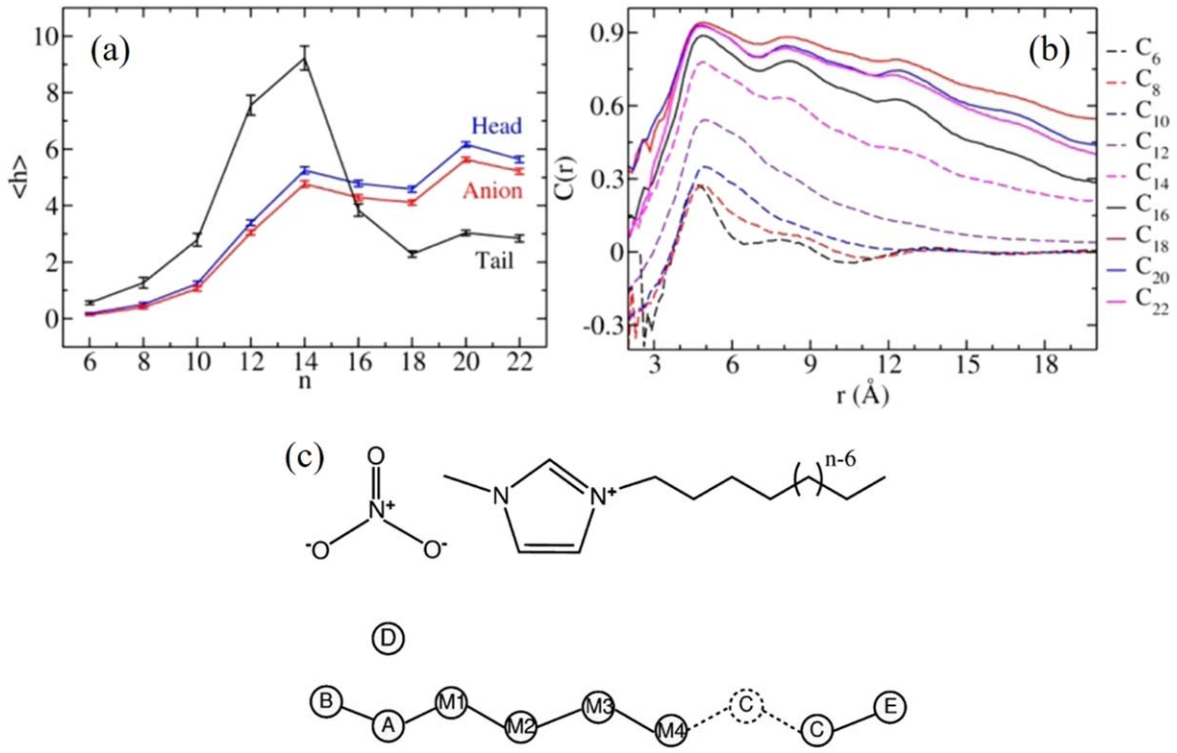

Figure 4. (a) HOP for cationic head groups, anions, and cationic tail groups. (b) OCF for side chains. (c) Molecular structure of the investigated IL system and the corresponding coarse-grained model. Reprinted with permission from [81]. Copyright 2013 American Chemical Society.

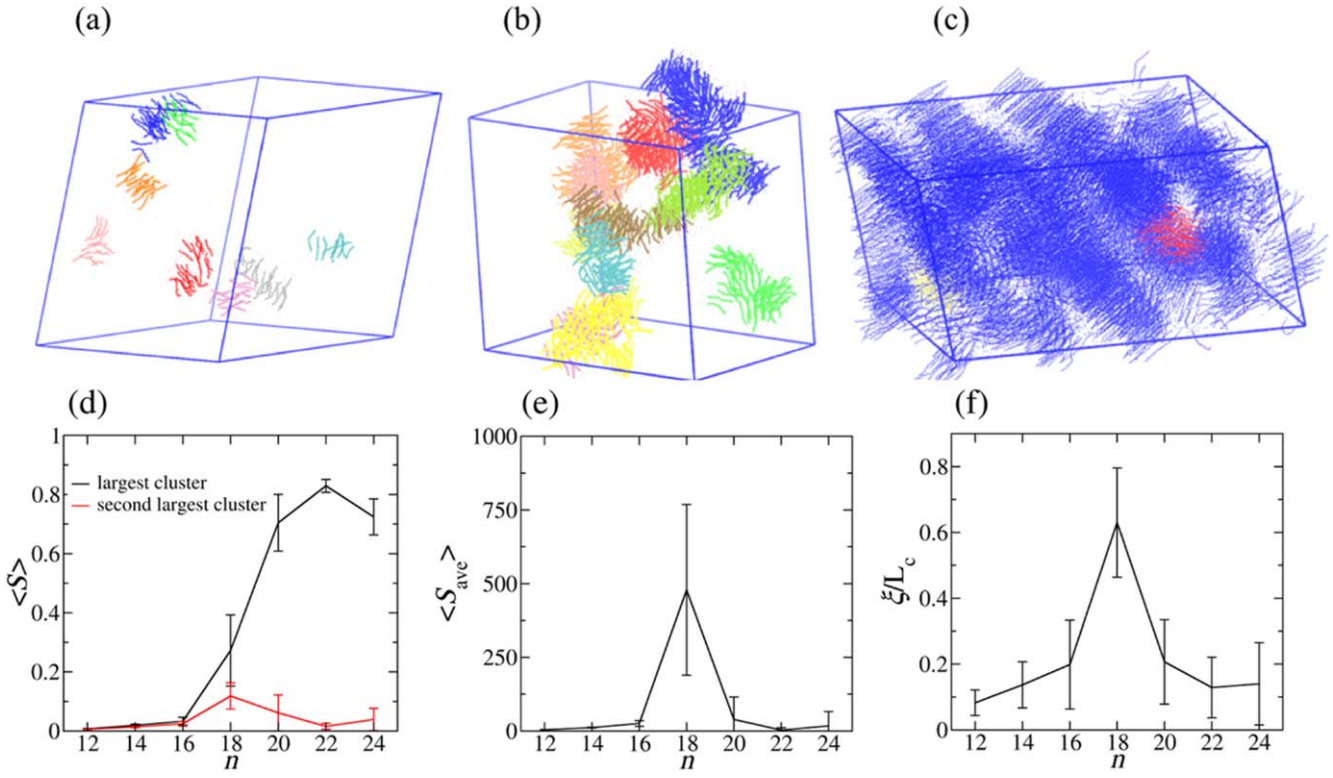

Figure 5. Percolation phase transition. (a)–(c) Several largest clusters in C_{12}, C_{16} and C_{22} systems, respectively, with the largest cluster colored blue. (a) The largest cluster in C_{12} is very small and not well aligned. (b) The largest cluster in C_{16} is larger and better aligned in parallel, but still local with little orientation correlation between clusters. (c) The largest cluster in C_{22} almost fills in the whole simulation box, indicating that the majority of the side chains are globally aligned in parallel and well connected. (d) Normalized sizes of the largest and second-largest clusters for all systems. (e) Average cluster size versus side-chain length. After the percolation phase transition, the largest cluster is not counted in the calculation of the average cluster size. (f) Correlation length versus side-chain length. For a finite system, both the average cluster size and the correlation length reach their maxima at the phase transition point. The correlation length is directly related to the average cluster size. Reprinted with permission from [116].

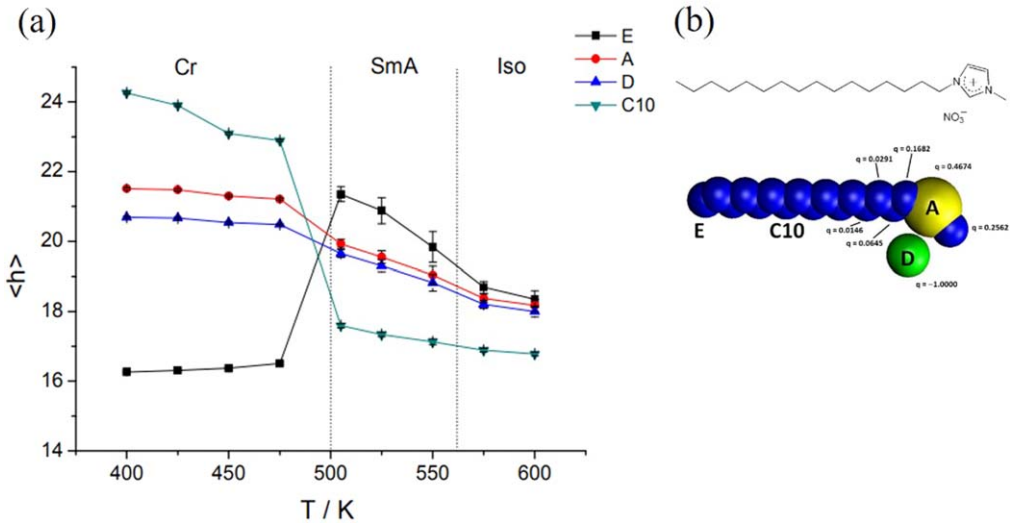

Figure 6. HOPs for some CG sites as a function of temperature. The error bars are almost invisible since they are smaller than the size of the markers. Cr represents the crystal phase, SmA the smectic A phase, and Iso the NSL phase. Reprinted with permission from [119]. Copyright 2015 American Chemical Society.

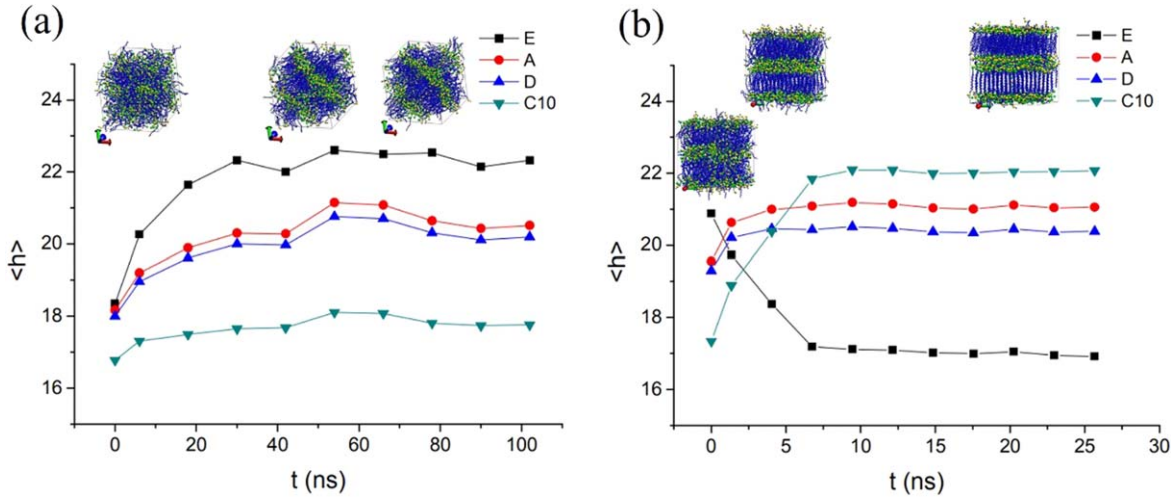

Figure 7. (a) HOP values for some CG sites as a function of time during the transition from the NSL phase into the smectic A phase, along with snapshots taken at $T = 505$ K after simulated for 0, 48, and 72 ns. (b) HOP values for some CG sites as a function of time during the transition from the smectic A phase into the crystal phase, along with snapshots taken at $T = 480$ K after simulated for 0, 5, and 20 ns. Reprinted with permission from [119]. Copyright 2015 American Chemical Society.

their maxima of around 500 and 0.42, respectively, with large fluctuations (figures 5(e) and (f)).

In the above simulations, although a CG model has been adopted, the simulated IL systems still suffer from limited equilibration time and finite-size effects. Therefore, the above results render future studies with even larger temporal and spatial simulation scales to refine the microscopic mechanism of the phase transition in ILs from the NSL state to the ILC state.

5. Solid–solid and melting phase transitions

Apart from varying side-chain lengths of the ILs, it has also been observed in computational and experimental studies that phase transitions can exist when varying temperatures or artificially tuning partial charges of ions [119, 120]. By MD simulations with the EF-CG model conducted on $[C_{16}MIm][NO_3]$, Saielli *et al* [119] have discovered that, with increasing temperature, the phase of IL can transit firstly from crystalline to smectic A (SmA) ILC, and then from ILC to NSL, which is similar to experimental results conducted on $[C_nMIm][BF_4]$ [80, 121]. The HOP provides direct evidence for the existence of such transitions since the HOP of the tail groups (CG sites E) increases drastically between 470 K and 505 K, corresponding to the phase transition from crystal to ILC, and decreases after 550 K, from ILC to NSL (figure 6). The snapshots representing the development from ILC to crystal at 480 K and from NSL to ILC at 550 K, respectively, are illustrated in figure 7.

Similar phase behavior can also be observed while tuning partial charges [120]. The phase transitions are observed and

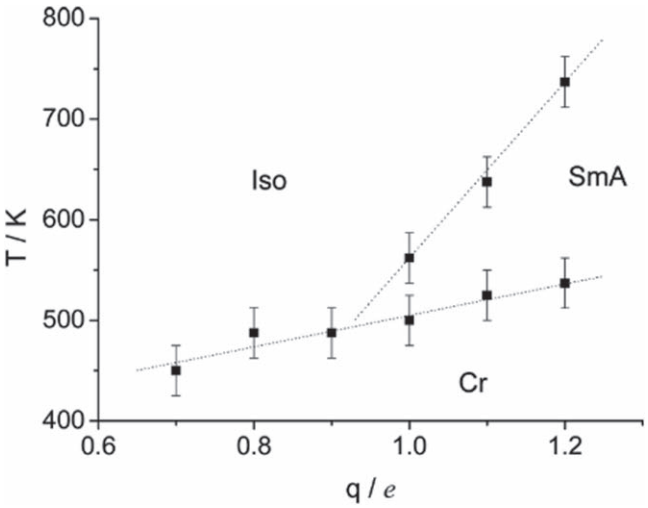

Figure 8. Phase diagram of the IL system simulated with the EF-CG model. Cr represents the crystal phase, SmA the smectic A phase, and Iso the NSL phase. Reprinted with permission from [120]. Copyright 2016 American Chemical Society.

determined by calculating the orientational order parameter (OOP) and the translational order parameter (TOP), which are commonly used in describing the LC phase transitions. It is thus possible for the phase diagram to be determined as a function of temperature and partial charges (figure 8). This study suggests that the existence of the ILC phases is strongly increased by the total charge of the ions. When the partial charges on the CG sites are rescaled by a factor lower than 0.9, the ILC phase is absent and the crystal directly melts into the NSL phase. For the systems with larger partial charges, the thermal range for a stable ILC phase is significantly increased. The HOP of the NSL phase also suggests that the nanoscale segregation is largely affected by the partial charges: the IL systems tend to be homogenous with low partial charges while nanosegregate with larger partial charges. The IL systems melted from the ILC phase have a higher degree of nanosegregation, as measured by the HOP, than that melted directly from the crystal at the same temperature. These studies indicate that the increase of either the alkyl chain length or the total charge of the cation head group and anion intensifies the competition between hydrophobic and electrostatic interactions, which enlarges the existence ranges on the phase diagram for both the NSL phase and the ILC phase.

Cao *et al* [84] have investigated the phase behavior of $[C_n\text{MIm}][NO_3]$ $(n = 4 - 12)$ during heating by manually constructing the initial crystal structures that constitute parallel polar layers composed of cationic head groups and anions as well as nonpolar regions composed of cationic alkyl side chains in between. The initial configuration is then heated by all-atom MD simulation with the AMBER force field.

During the heating process, a solid–solid phase transition has been found below the melting point, manifested by the kinks on the caloric curves shown in figure 9. The jumps of the potential energies at the solid–solid phase transition points are much smaller than those at melting transition points. The C_4 system exhibits distinctiveness compared with others due to its weaker VDW interaction coming from the shorter side chains. The difference between such phase transitions of C_4 and C_8 is shown in figure 10. The TOPs and OOPs indicate that the conformations of alkyl chains of the C_4 system are not as ordered as those with longer side chains.

Further increasing the simulation temperature indicates that the melting phase transition of the investigated systems consists of two steps except for C_6, which has only one step. A metastable state exhibits during the melting transition when the crystalline solid phase is transformed into the NSL phase (for C_4, C_6, and C_8) or SmA ILC phase (for C_{10} and C_{12}). The snapshots of the metastable states of C_4 and C_8 systems are shown in figure 9(b). The metastable state tends to be more stable along with a higher melting temperature when the alkyl chain becomes longer. These features of melting transitions can be comprehended by the competition between the free energy contributions of the effective VDW interaction in the nonpolar regions (or EF1 for abbreviation) and that of the effective electrostatic interaction in the polar layers (or EF2 for abbreviation). The existence of the unique solid–solid phase behavior of ILs can thus be attributed to the dual ionic and organic nature of ILs.

As the side-chain length increases, EF1 becomes stronger and thus the system possesses ordered conformations during solid–solid phase transitions. During the melting process, the imbalance between EF1 and EF2 at the melting point leads to an uneven melting process of polar layers and nonpolar regions, which causes the metastable phase to appear. For the C_4 system, EF1 is weaker than EF2 at the melting point of 315 K, so the alkyl side chains lose the crystalline order before the polar layers do. For systems containing C_8 to C_{12}, longer alkyl side chains lead to stronger EF1, and thus the increase of the melting temperatures, at which the alkyl side chains keep their orientations uniformly for a certain time whilst polar layers drift from their original lattice positions. For the C_6 system, the free energy contributions from the two interactions are well balanced, resulting in the absence of the metastable phase.

The above phase transition in $[C_n\text{MIm}][NO_3]$ ($n = 2$, 4, 6, 8, and 10) systems was later experimentally examined by Abe *et al* [122]. In particular, they examined the phase transition of $[C_{10}\text{mim}][NO_3]$ via simultaneous SWAXS and DSC measurements, which indicate the existence of a multistep phase transition process.

6. Partially arrested glassy state

The self-consistent generalized Langevin equation (SCGLE) theory has been used to investigate the dynamics of molten salts, and such implementation has predicted the existence of the so-called partially arrested state when the larger ions are still in the fluid state while the smaller counter-ions are arrested in the glassy state [123]. The SCGLE theory puts forward a simple equation for the asymptotic value of the mean-squared displacement of species α, which is defined as $\gamma_\alpha \equiv \lim_{t\to\infty} \langle(\Delta R^{(\alpha)})^2\rangle$, and the equation reads as [124]:

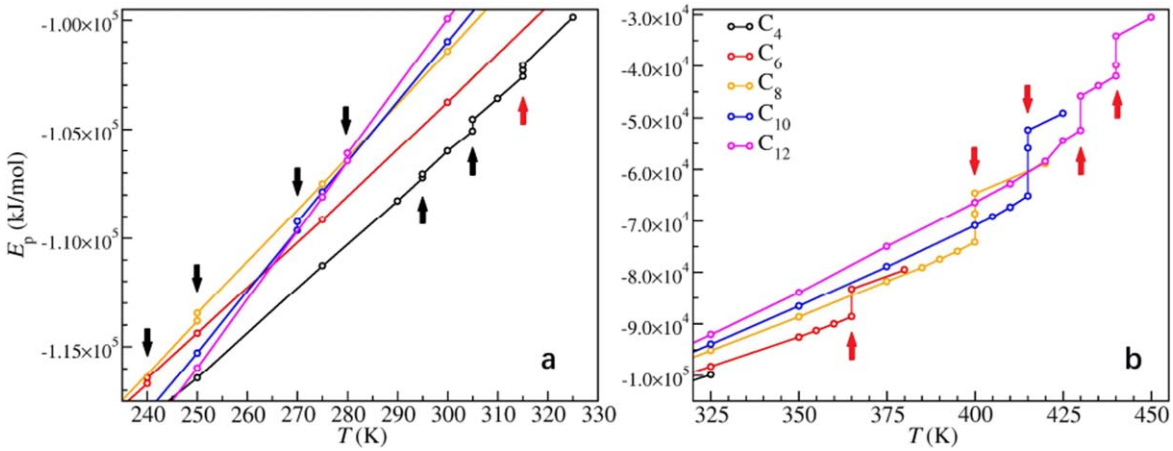

Figure 9. Caloric curves during heating in $[C_n MIm][NO_3]$ systems. (a) From $T = 240$ K to 325 K. (b) From $T = 325$ K to 450 K. The solid–solid phase transition points are marked by black arrows, and the melting transition points are marked by red arrows. Reprinted with permission from [84]. Copyright 2018 American Chemical Society.

$$\frac{1}{\gamma_\alpha} = \frac{1}{3(2\pi)^3}\int \mathrm{d}^3 k k^2 \{\lambda[\lambda + k^2\gamma]^{-1}\}_{\alpha\alpha} \times \{c\sqrt{n}S\lambda[S\lambda + k^2\gamma]^{-1}\sqrt{n}h\}_{\alpha\alpha}, \quad (4)$$

where S is the matrix of partial structure factors, h and c are the Ornstein-Zernike matrices of total and direct correlation functions, respectively, and $\{...\}_{\alpha\alpha}$ represents the diagonal elements of the matrices. The matrix $\sqrt{n}$ is defined as $[\sqrt{n}]_{\alpha\beta} \equiv \delta_{\alpha\beta}\sqrt{n_\alpha}$, where $\delta_{\alpha\beta} = 0$, $\alpha \neq \beta$; $\delta_{\alpha\beta} = 1$, $\alpha = \beta$ and $\lambda(k)$ as $\lambda_{\alpha\beta}(k) = \delta_{\alpha\beta}[1 + (k/k_c^{(\alpha)})^2]^{-1}$ where $k_c^{(\alpha)} = 8.17/\sigma_\alpha$ with σ_α being the diameter of the investigated particle and k being the wave factor. The theoretical prediction for molten salts indicates that there are partially arrested states in the dynamic arrest line (F–G region in figure 11(a)) where only one species of ions are arrested in the glassy state while the counter-ions are still in the liquid state.

Ramírez-Gonzalez *et al* [83] have applied the SCGLE theory to investigating the $[C_2MIm][BF_4]$ IL and found that the IL system is very likely to be in the partially arrested glassy state. Anions' value $\gamma_{\mathrm{anion}}^{-1}$ varies from zero at higher temperatures than cations' value $\gamma_{\mathrm{cation}}^{-1}$, which suggests that the IL is in the F–G region with the anions arrested while the cations being liquid. As a consequence, although at short times, the mobility of BF_4^- is higher than that of C_2MIm^+ due to the free flight in the ballistic regime, it is observed that the diffusion of the smaller BF_4^- becomes slower than the larger C_2MIm^+ in the diffusive regime, as observed in the all-atom MD simulations with the Amber force field [21] (figure 11(b)). By analyzing the RDFs between cations and anions, Ramírez-Gonzalez and co-workers have discovered that the anions behave as a typical Wigner glass whose mean distance of the constituents is very large.

7. Liquid–liquid phase separation of IL/benzene mixture

Aside from pure IL systems, the phase behaviors of IL mixtures have also attracted much attention. Specifically, since ILs are found to exhibit dual ionic and organic nature and amphiphilic features, the mixtures of ILs and organic molecules have been widely investigated [125–133]. Unlike ILs directly solved in many small organic solvents, such as acetonitrile, dichloromethane, and chloroform [134], ILs mixed with benzene exhibit liquid–liquid phase separation. Holbrey *et al* [128] observed experimentally that aromatic molecules, such as benzene and toluene, are soluble in imidazolium-based ILs and that liquid–liquid phase separations occur in the mixtures of ILs and aromatic liquids. Later studies on the solubility of aromatic molecules in different ILs also indicate that electrostatic interactions between cations and anions can be of much decisiveness in understanding the phase separation [125, 126, 130–133].

To understand the microscopic mechanisms of the above liquid–liquid phase separation, Li *et al* [135] performed both NMR experiments and all-atom MD simulations on a set of mixtures of benzene and viologen bistriflimide salts $[C_m(bpC_n)_2][CF_3(SO_2)_2N]$ with m and n being the numbers of carbon atoms on the two alkyl side chains. The viologen salts are crystal at room temperature but also exhibit ILC and NSL phases at higher temperatures, as common ILs do [135].

Both NMR experiments and MD simulations confirm that, when mixed with benzene, the salt absorbs benzene molecules to form a sponge-like phase with benzene inserted in the nonpolar domains of the NSL-like structure compose of nonpolar alkyl chains surrounded by the continuous polar network formed by anions and charged cationic head groups (figure 12(b)). This mixture phase coexists with liquid benzene or crystalline viologen-based IL whichever is excessive. The upper boundaries separating the coexisting phases depend linearly on the cationic alkyl chain length of the IL (figure 12(a)) because a larger volume of nonpolar domains can absorb more benzene molecules. The lower boundaries also exhibit linear dependency on the side-chain length corresponding to the minimum amount of benzene required to liquidize the salt, which increases proportionally with the cationic side-chain length.

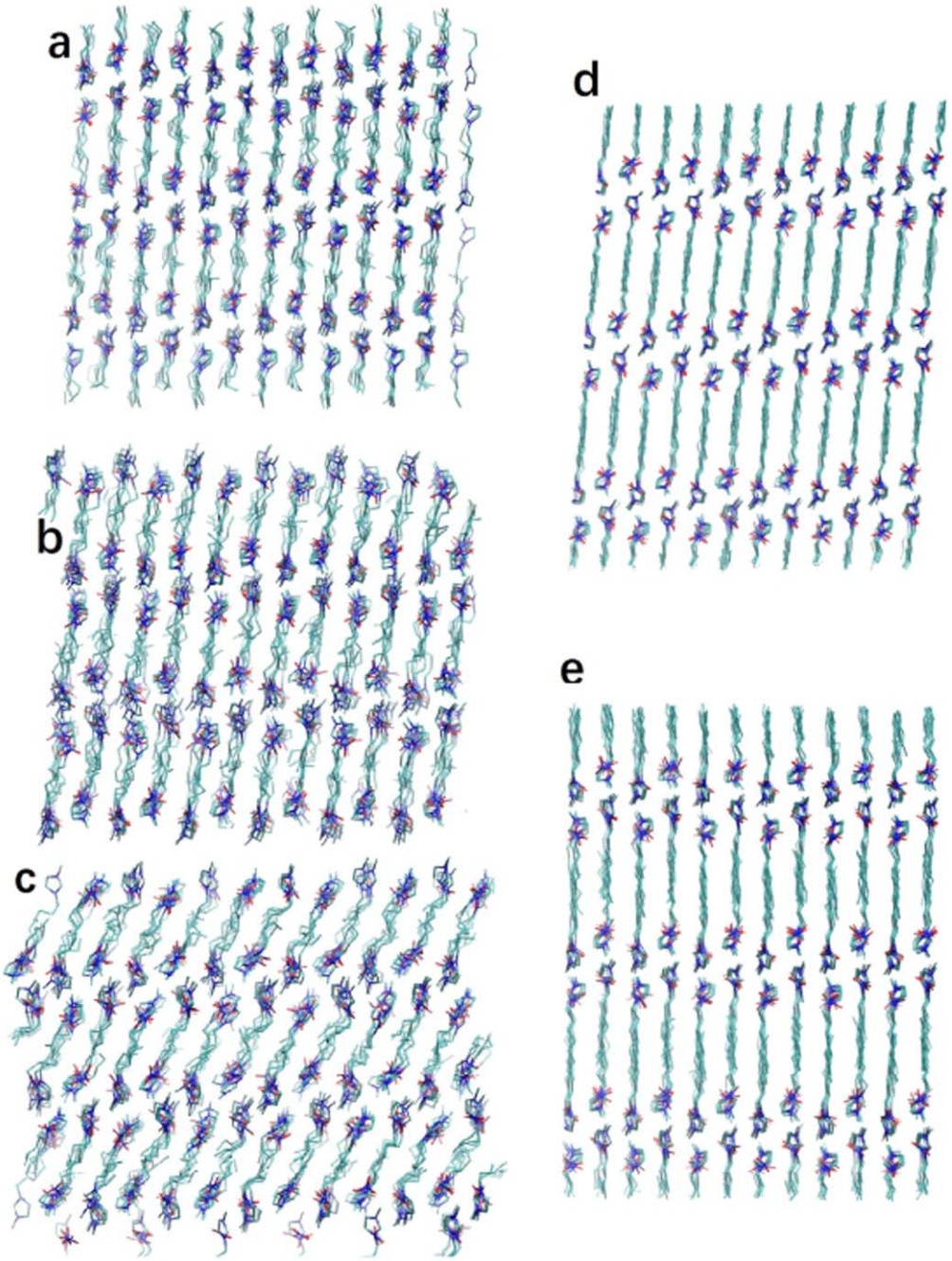

Figure 10. Snapshots of the structures before and after the solid–solid phase transitions. (a) C_4 at 295 K before the phase transition. (b) C_4 at 300 K after the first but before the second phase transition. (c) C_4 at 305 K after the phase transition. (d) C_8 at 250 K before the phase transition. (e) C_8 at 250 K after the phase transition. All these snapshots are taken from the [100] direction. Reprinted with permission from [84]. Copyright 2018 American Chemical Society.

Although many other investigations [125, 126, 128, 131, 133] have suggested that π–π or ion-π interactions between cations and benzene molecules may contribute to such kind of liquid–liquid phase separations, the MD simulations have indicated that they do not exist in the above benzene/viologen-based IL mixture systems, and the benzene molecules reside inside the nonpolar domains only due to their planar and nonpolar molecular feature. Further studies in this direction may investigate the influence of the alkyl chain length, the cation and anion types, and the temperature on the liquid–liquid phase separation behaviors of the mixtures composed of various ILs and small organic molecules and develop a general theoretical framework for this kind of phase behaviors.

8. Other phase behaviors of ILs

ILs mixed with water constitute an important topic of investigation. Many MD simulations on the mixtures of water with imidazolium-based ILs have focused on studying their structural characteristics, analyzing the RDFs and spatial

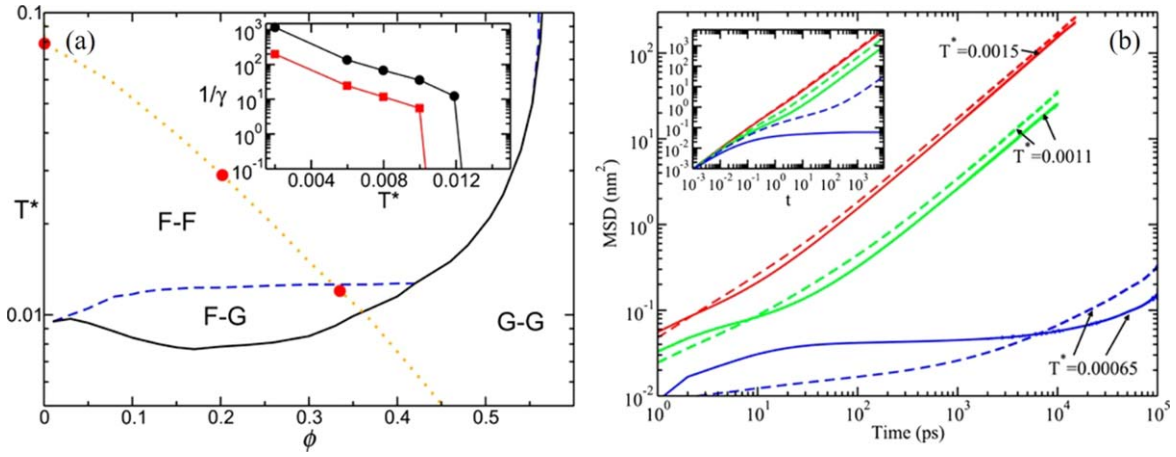

Figure 11. (a) Arrest lines predicted by the SCGLE theory for the primitive model with a size asymmetry adequate for the simulated IL (1:3.5). The fluid region is labelled as F–F. The G–G region corresponds to fully arrested states. The partially arrested phenomenon occurs in the F–G region. The inset shows the values of the parameter $1/\gamma\alpha$ following the isobaric trajectory with a pressure of 1 atm indicated by the dotted line. Circles correspond to anions (smaller particles) and squares to cations (larger particles). (b) MSDs for [EMIM][BF_4]. Dashed lines represent cations and solid lines represent anions. The inset shows the theoretical calculation results of the MSDs over the isobaric trajectory (big circles in the left panel). The first two temperatures are located in the F–F region and the last one inside the F–G region. Solid and dashed lines correspond to anions and cations, respectively. Reprinted from [83] with permission from AIP Publishing.

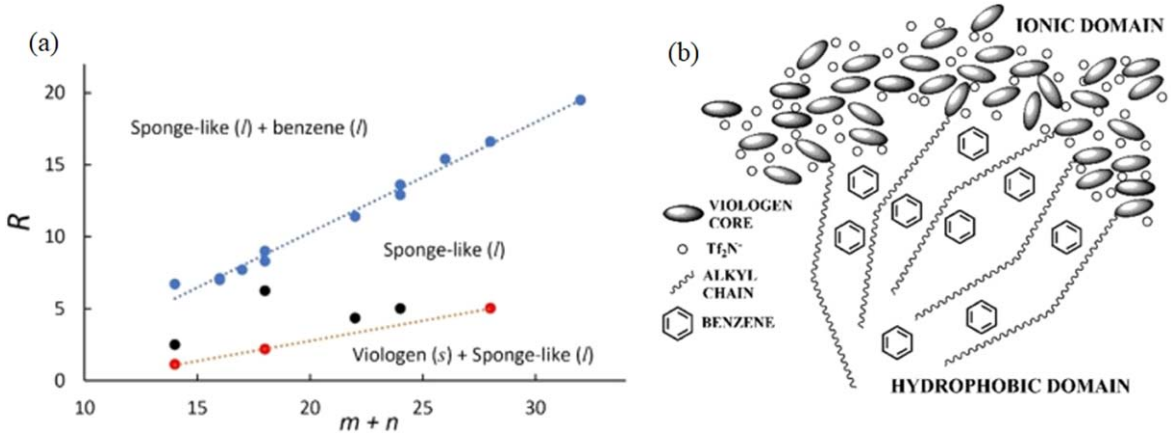

Figure 12. (a) Phase diagram of the mole ratio $R = N_{\text{benzene}}/N_{\text{viologen}}$ versus $m + n$, the total number of carbon groups in the cationic alkyl chains, measured by experiment. The blue symbols represent the coexistence line between liquid benzene and sponge-like liquid phase, the red symbols represent the coexistence line between solid viologen salt and sponge-like liquid phase, and the black symbols represent intermediate state points with only the sponge-like liquid phase present. (b) Schematic representation of the sponge-like phase. The typical nanoscale segregation normally observed in ionic liquids is reproduced in the sponge-like phase after benzene molecules are absorbed in the hydrophobic regions. For the sake of clarity, only a few alkyl chains are schematically drawn. Reprinted with permission from [135]. Copyright 2020 American Chemical Society.

distribution functions (SDFs), whereas many others have focused majorly on depicting the mixture by analyzing hydrogen bonds or investigating the effect of alkyl chain length on their dynamics [136–146]. Some investigators have also addressed the significance of unique structural features. Jiang *et al* [147] studied the influence of water molecules on the NSL structure of [C_8MIm][NO_3], and water molecules were found to be inserted inside the polar network of the IL. Abe and coworkers [148–151] further determined the existence of aggregations of water molecules in IL systems by discovering the percolation limit that Bernardes *et al* [152] predicted through MD simulations. They also brought up a hypothesis that the so-called 'water pockets' exist in the mixture. Bystrov *et al* [136] have confirmed the existence of nanoscale structures in IL/water mixtures. By using MD simulation and the experimental Pulsed Field Gradient-Stimulated Echo method, they have discovered that other than forming 'water pockets' or 'nanodroplets', water molecules tend to distribute within the hydrophilic region in the IL system. All of these studies indicate that the NSL structure of ILs plays an important role in the mixture of IL and water.

Another set of mixing systems undergoing intense investigations is the binary IL mixtures. It has been widely accepted that, by varying cationic head groups, their side-chain length, and the nature of anions, the NSL structures of ILs can be fine-tuned [103, 107, 153–155]. There is, however, an alternative option of mixing two or more types of ILs with different chemical structures [156]. Cosby *et al* [157] have

thoroughly studied how tuning the composition of binary IL mixtures can affect the mesoscale organization and dynamics of the mixing system with the example of $[C_8MIm][BF_4]$ and $[C_2MIm][BF_4]$ mixture. Through detailed x-ray scattering, neutron scattering, and MD simulation studies, Cosby has discovered that increasing the mole ratio of $[C_2MIm][BF_4]$ can lead to the increase of static dielectric permittivity, ε_s, which is the consequence of a transition in the mesoscale morphologies of the binary mixing system.

Unique phase separation behaviors are observed in many other mixing systems as well. In a computational study of a ternary electrolyte mixture of tetramethylene glycol dimethyl ether (tetraglymeor G_4), $[C_2MIm][BF_4]$, and Li salts ($LiNO_3$ and LiI), Fuladi *et al* [158] have discovered that resembling the phase separation of IL mixtures, the ternary mixture tends to separate into two domains with one majorly consisted of ionic species and the other consisted of only G_4 molecules. This phase separation has been analyzed by changing the volume fraction of G_4 and ILs, salt concentration, and temperature. It is believed that the phase separation process is driven primarily by entropy and is thus temperature sensitive, which slows the diffusive dynamics of Li^+ ions. This study will inspire future investigation and engineering of IL electrolytes that may improve the performance of Li batteries.

9. Conclusions

ILs are room-temperature organic salts that possess both ionic and organic characteristics, which leads to some distinctive phase behaviors both in the context of pure ILs and their mixture with other liquids. Previous theoretical, computational, and experimental studies on phase behaviors of ILs have suggested the existence of many phases in this amphiphilic liquid, whose phase behaviors can be fine-tuned by manipulating thermodynamic conditions and molecular structures, such as charge distribution, length of cationic alkyl side chains, and temperature. Mixing with other molecules can vary their phase behaviors as well.

With an intermediate alkyl cationic side-chain length, ILs exhibit a unique NSL state which is macroscopically isotropic but microscopically phase-separated into a polar network and nonpolar domains. The ILC phase appears when the alkyl side chains are sufficiently long. For the crystalline solid of ILs, when increasing temperature, the solid–solid phase transition may occur and the melting transition from crystal to IL or ILC sometimes encounters a metastable state. At a certain thermal condition, an IL system may stay in the partially arrested glassy state. Liquid–liquid phase separation can occur when ILs mixed with some sorts of small organic molecules.

By increasing alkyl side-chain length, ILs go over a percolation phase transition from the NSL phase to the ILC phase due to the increasing VDW interactions among alkyl side chains to transform the conformation of side-chain bundles from nanoscale aggregation to globally parallel alignment. Most of the phase behaviors of aprotic ILs can be qualitatively understood by the competition between the effective free energy contributions from the collective VDW interactions among alkyl side chains and the electrostatic interactions among charged anions and cationic head groups.

It can be noted that the dual ionic and organic nature of ILs plays an important role in determining the unique phase behaviors of ILs. The studies mentioned in this review thus pave the way for future theoretical works investigating phase behaviors of ILs and their mixtures from this perspective. Through analyzing the free energy contributions from electrostatic and VDW interactions, analytical models may be viable to provide a unified mechanism to explain the existing computational and experimental results and provide researchers and engineers with proper guidance to finely tune the physical and chemical properties of ILs in favor of certain industrial applications.

Acknowledgments

This work was supported by the National Natural Science Foundation of China (Nos. 11774357, 22011530390, 12047503) and the Chinese Academy of Sciences (No. QYZDJ-SSW-SYS01).

ORCID iDs

Yanting Wang (王延颋) https://orcid.org/0000-0002-0474-4790

References

[1] Rogers R D and Seddon K R 2003 Ionic liquids–solvents of the future? *Science* **302** 792
[2] Wilkes J S and Zaworotko M J 1992 Air and water stable 1-ethyl-3-methylimidazolium based ionic liquids *J. Chem. Soc., Chem. Commun.* 965
[3] Wilkes J S 2002 A short history of ionic liquids—from molten salts to neoteric solvents *Green Chem.* **4** 73
[4] Armand M, Endres F, MacFarlane D R, Ohno H and Scrosati B 2009 Ionic-liquid materials for the electrochemical challenges of the future *Nat. Mater.* **8** 621
[5] Pârvulescu V I and Hardacre C 2007 Catalysis in ionic liquids *Chem. Rev.* **107** 2615
[6] Plechkova N V and Seddon K R 2008 Applications of ionic liquids in the chemical industry *Chem. Soc. Rev.* **37** 123
[7] Somers A E, Howlett P C, MacFarlane D R and Forsyth M 2013 A review of ionic liquid lubricants *Lubricants* **1** 3
[8] Torimoto T, Tsuda T, Okazaki K I and Kuwabata S 2010 New frontiers in materials science opened by ionic liquids *Adv. Mater.* **22** 1196
[9] Van Rantwijk F and Sheldon R A 2007 Biocatalysis in ionic liquids *Chem. Rev.* **107** 2757
[10] Welton T 1999 Room-temperature ionic liquids. Solvents for synthesis and catalysis *Chem. Rev.* **99** 2071
[11] Bhargava B, Balasubramanian S and Klein M L 2008 Modelling room temperature ionic liquids *Chem. Commun.* 3339
[12] Hunt P 2006 The simulation of imidazolium-based ionic liquids *Mol. Simul.* **32** 1
[13] Lynden-Bell R M, Del Popolo M G, Youngs T G, Kohanoff J, Hanke C G, Harper J B and Pinilla C C 2007 Simulations of

ionic liquids, solutions, and surfaces *Acc. Chem. Res.* **40** 1138
[14] Kelkar M S and Maginn E J 2007 Effect of temperature and water content on the shear viscosity of the ionic liquid 1-ethyl-3-methylimidazolium bis (trifluoromethanesulfonyl) imide as studied by atomistic simulations *J. Phys. Chem.* B **111** 4867
[15] Plimpton S 1995 Fast parallel algorithms for short-range molecular dynamics *J. Comput. Phys.* **117** 1
[16] Berendsen H J, van der Spoel D and van Drunen R 1995 GROMACS: a message-passing parallel molecular dynamics implementation *Comput. Phys. Commun.* **91** 43
[17] Phillips J C *et al* 2005 Scalable molecular dynamics with NAMD *J. Comput. Chem.* **26** 1781
[18] Canongia Lopes J N, Deschamps J and Pádua A A 2004 Modeling ionic liquids using a systematic all-atom force field *J. Phys. Chem.* B **108** 2038
[19] Wang Y, Pan H, Li H and Wang C 2007 Force field of the TMGL ionic liquid and the solubility of SO_2 and CO_2 in the TMGL from molecular dynamics simulation *J. Phys. Chem.* B **111** 10461
[20] Bhargava B and Balasubramanian S 2007 Refined potential model for atomistic simulations of ionic liquid [bmim][PF_6] *J. Chem. Phys.* **127** 114510
[21] Wang J, Wolf R M, Caldwell J W, Kollman P A and Case D A 2004 Development and testing of a general amber force field *J. Comput. Chem.* **25** 1157
[22] Jorgensen W L, Maxwell D S and Tirado-Rives J 1996 Development and testing of the OPLS all-atom force field on conformational energetics and properties of organic liquids *J. Am. Chem. Soc.* **118** 11225
[23] Vanommeslaeghe K *et al* 2010 CHARMM general force field: a force field for drug-like molecules compatible with the CHARMM all-atom additive biological force fields *J. Comput. Chem.* **31** 671–90
[24] Bagno A, D'Amico F and Saielli G 2007 Computer simulation of diffusion coefficients of the room-temperature ionic liquid [bmim][BF_4]: problems with classical simulation techniques *J. Mol. Liq.* **131** 17
[25] Bhargava B and Balasubramanian S 2006 Intermolecular structure and dynamics in an ionic liquid: a Car–Parrinello molecular dynamics simulation study of 1, 3-dimethylimidazolium chloride *Chem. Phys. Lett.* **417** 486
[26] Bhargava B and Balasubramanian S 2005 Dynamics in a room-temperature ionic liquid: a computer simulation study of 1, 3-dimethylimidazolium chloride *J. Chem. Phys.* **123** 144505
[27] Bhargava B L, Klein M L and Balasubramanian S 2008 Structural correlations and charge ordering in a room-temperature ionic liquid *ChemPhysChem* **9** 67
[28] Canongia Lopes J N, Pádua A A and Shimizu K 2008 Molecular force field for ionic liquids IV: trialkylimidazolium and alkoxycarbonyl-imidazolium cations; alkylsulfonate and alkylsulfate anions *J. Phys. Chem.* B **112** 5039
[29] Denesyuk N A and Weeks J D 2008 A new approach for efficient simulation of Coulomb interactions in ionic fluids *J. Chem. Phys.* **128** 124109
[30] Lynden-Bell R and Youngs T 2006 Using DL_POLY to study the sensitivity of liquid structure to potential parameters *Mol. Simul.* **32** 1025
[31] Micaelo N M, Baptista A M and Soares C M 2006 Parametrization of 1-butyl-3-methylimidazolium hexafluorophosphate/nitrate ionic liquid for the GROMOS force field *J. Phys. Chem.* B **110** 14444
[32] Schröder C and Steinhauser O 2008 The influence of electrostatic forces on the structure and dynamics of molecular ionic liquids *J. Chem. Phys.* **128** 224503
[33] Youngs T G, Del Pópolo M G and Kohanoff J 2006 Development of complex classical force fields through force matching to ab initio data: Application to a room-temperature ionic liquid *J. Phys. Chem.* B **110** 5697
[34] Youngs T G and Hardacre C 2008 Application of static charge transfer within an ionic-liquid force field and its effect on structure and dynamics *ChemPhysChem* **9** 1548
[35] Yan T, Burnham C J, Del Pópolo M G and Voth G A 2004 Molecular dynamics simulation of ionic liquids: The effect of electronic polarizability *J. Phys. Chem. B* **108** 11877
[36] Yan T, Wang Y and Knox C 2010 On the structure of ionic liquids: comparisons between electronically polarizable and nonpolarizable models I *J. Phys. Chem.* B **114** 6905
[37] Yan T, Wang Y and Knox C 2010 On the dynamics of ionic liquids: comparisons between electronically polarizable and nonpolarizable models II *J. Phys. Chem.* B **114** 6886
[38] Izvekov S, Violi A and Voth G A 2005 Systematic coarse-graining of nanoparticle interactions in molecular dynamics simulation *J. Phys. Chem.* B **109** 17019
[39] Izvekov S and Voth G A 2005 Multiscale coarse graining of liquid-state systems *J. Chem. Phys.* **123** 134105
[40] Izvekov S and Voth G A 2005 A multiscale coarse-graining method for biomolecular systems *J. Phys. Chem.* B **109** 2469
[41] Wang Y, Feng S and Voth G A 2009 Transferable coarse-grained models for ionic liquids *J. Chem. Theory Comput.* **5** 1091
[42] Wang Y, Noid W G, Liu P and Voth G A 2009 Effective force coarse-graining *Phys. Chem. Chem. Phys.* **11** 2002
[43] Del Pópolo M G, Kohanoff J and Lynden-Bell R M 2006 Solvation structure and transport of acidic protons in ionic liquids: a first-principles simulation study *J. Phys. Chem.* B **110** 8798
[44] Del Pópolo M G, Lynden-Bell R M and Kohanoff J 2005 *Ab initio* molecular dynamics simulation of a room temperature ionic liquid *J. Phys. Chem.* B **109** 5895
[45] Ghatee M H and Ansari Y 2007 *Ab initio* molecular dynamics simulation of ionic liquids *J. Chem. Phys.* **126** 154502
[46] Banks J L, Kaminski G A, Zhou R, Mainz D T, Berne B and Friesner R A 1999 Parametrizing a polarizable force field from ab initio data. I. The fluctuating point charge model *J. Chem. Phys.* **110** 741
[47] Bedrov D, Piquemal J-P, Borodin O, MacKerell A D Jr, Roux B and Schröder C 2019 Molecular dynamics simulations of ionic liquids and electrolytes using polarizable force fields *Chem. Rev.* **119** 7940–95
[48] Chelli R, Procacci P, Righini R and Califano S 1999 Electrical response in chemical potential equalization schemes *J. Chem. Phys.* **111** 8569
[49] Chen J, Hundertmark D and Martínez T J 2008 A unified theoretical framework for fluctuating-charge models in atom-space and in bond-space *J. Chem. Phys.* **129** 214113
[50] Olano L R and Rick S W 2005 Fluctuating charge normal modes: An algorithm for implementing molecular dynamics simulations with polarizable potentials *J. Comput. Chem.* **26** 699
[51] Patel S and Brooks C L III 2006 Fluctuating charge force fields: recent developments and applications from small molecules to macromolecular biological systems *Mol. Simul.* **32** 231
[52] Rick S W and Stuart S 2003 Potentials and algorithms for incorporating polarizability in computer simulations *Rev. Comput. Chem.* **18** 89
[53] Kohagen M, Brehm M, Thar J, Zhao W, Muller-Plathe F and Kirchner B 2011 Performance of quantum chemically derived charges and persistence of ion cages in ionic liquids. A molecular dynamics simulations study of 1-n-butyl-3-methylimidazolium bromide *J. Phys. Chem.* B **115** 693

[54] Bhargava B L, Devane R, Klein M L and Balasubramanian S 2007 Nanoscale organization in room temperature ionic liquids: a coarse grained molecular dynamics simulation study *Soft Matter* **3** 1395

[55] Karimi-Varzaneh H A, Muller-Plathe F, Balasubramanian S and Carbone P 2010 Studying long-time dynamics of imidazolium-based ionic liquids with a systematically coarse-grained model *Phys. Chem. Chem. Phys.* **12** 4714

[56] Merlet C, Salanne M and Rotenberg B 2012 New coarse-grained models of imidazolium ionic liquids for bulk and interfacial molecular simulations *J. Phys. Chem.* C **116** 7687

[57] Moradzadeh A, Motevaselian M H, Mashayak S Y and Aluru N R 2018 Coarse-grained force field for imidazolium-based ionic liquids *J. Chem. Theory Comput.* **14** 3252

[58] Salanne M 2015 Simulations of room temperature ionic liquids: from polarizable to coarse-grained force fields *Phys. Chem. Chem. Phys.* **17** 14270

[59] Vazquez-Salazar L I, Selle M, De Vries A H, Marrink S J and Souza P C 2020 Martini coarse-grained models of imidazolium-based ionic liquids: from nanostructural organization to liquid–liquid extraction *Green Chem.* **22** 7376

[60] Bresme F and Alejandre J 2003 Cavities in ionic liquids *J. Chem. Phys.* **118** 4134

[61] Shah J K, Brennecke J F and Maginn E J 2002 Thermodynamic properties of the ionic liquid 1-n-butyl-3-methylimidazolium hexafluorophosphate from Monte Carlo simulations *Green Chem.* **4** 112

[62] Shi W and Maginn E J 2008 Atomistic Simulation of the Absorption of Carbon Dioxide and Water in the Ionic Liquid 1-n-Hexyl-3-methylimidazolium Bis (trifluoromethylsulfonyl) imide ([hmim][Tf2N] *J. Phys. Chem.* B **112** 2045

[63] Izgorodina E I, Forsyth M and MacFarlane D R 2009 On the components of the dielectric constants of ionic liquids: ionic polarization? *Phys. Chem. Chem. Phys.* **11** 2452

[64] Izgorodina E I 2011 Towards large-scale, fully ab initio calculations of ionic liquids *Phys. Chem. Chem. Phys.* **13** 4189

[65] Santiago R S, Santos G R and Aznar M 2009 UNIQUAC correlation of liquid–liquid equilibrium in systems involving ionic liquids: the DFT–PCM approach *Fluid Phase Equilib.* **278** 54

[66] Tsuzuki S, Tokuda H, Hayamizu K and Watanabe M 2005 Magnitude and directionality of interaction in ion pairs of ionic liquids: relationship with ionic conductivity *J. Phys. Chem.* B **109** 16474

[67] Fujii K, Fujimori T, Takamuku T, Kanzaki R, Umebayashi Y and Ishiguro S-I 2006 Conformational equilibrium of bis (trifluoromethanesulfonyl) imide anion of a room-temperature ionic liquid: Raman spectroscopic study and DFT calculations *J. Phys. Chem.* B **110** 8179

[68] Janesko B G 2011 Modeling interactions between lignocellulose and ionic liquids using DFT-D *Phys. Chem. Chem. Phys.* **13** 11393

[69] Karu K, Ruzanov A, Ers H, Ivaništšev V, Lage-Estebanez I and Garcia de la Vega J M 2016 Predictions of physicochemical properties of ionic liquids with DFT *Computation* **4** 25

[70] Katsyuba S A, Zvereva E E, Vidiš A and Dyson P J 2007 Application of density functional theory and vibrational spectroscopy toward the rational design of ionic liquids *J. Phys. Chem. A* **111** 352

[71] Zhang Y, He H, Dong K, Fan M and Zhang S 2017 A DFT study on lignin dissolution in imidazolium-based ionic liquids *RSC Adv.* **7** 12670

[72] Chiappe C 2007 Nanostructural organization of ionic liquids: theoretical and experimental evidences of the presence of well defined local structures in ionic liquids *Monatsh. Chem.* **138** 1035

[73] Wang Y, Jiang W and Voth G A 2007 (Book Chapter) Spatial Heterogeneity in Ionic Liquids *Ionic Liquids IV: Not Just Solvents Anymore* ed J F Brennecke *et al* (Washington: American Chemical Society) p 272

[74] Wang Y and Voth G A 2005 Unique spatial heterogeneity in ionic liquids *J. Am. Chem. Soc.* **127** 12192

[75] Wang Y and Voth G A 2006 Tail aggregation and domain diffusion in ionic liquids *J. Phys. Chem.* B **110** 18601

[76] Zhao H, Shi R and Wang Y 2011 Nanoscale tail aggregation in Ionic liquids: roles of electrostatic and van der Waals Interactions *Commun. Theor. Phys.* **56** 499

[77] Casella G, Causin V, Rastrelli F and Saielli G 2016 Ionic liquid crystals based on viologen dimers: tuning the mesomorphism by varying the conformational freedom of the ionic layer *Liq. Cryst.* **43** 1161

[78] Casella G, Causin V, Rastrelli F and Saielli G 2014 Viologen-based ionic liquid crystals: induction of a smectic a phase by dimerisation *Phys. Chem. Chem. Phys.* **16** 5048

[79] Gordon C M, Holbrey J D, Kennedy A R and Seddon K R 1998 Ionic liquid crystals: hexafluorophosphate salts *J. Mater. Chem.* **8** 2627

[80] Holbrey J D and Seddon K R 1999 The phase behaviour of 1-alkyl-3-methylimidazolium tetrafluoroborates; ionic liquids and ionic liquid crystals *J. Chem. Soc., Dalton Trans.* 2133

[81] Ji Y, Shi R, Wang Y and Saielli G 2013 Effect of the chain length on the structure of ionic liquids: From spatial heterogeneity to ionic liquid crystals *J. Phys. Chem.* B **117** 1104

[82] Lee C K, Huang H W and Lin I J 2000 Simple amphiphilic liquid crystalline N-alkylimidazolium salts. *Chem. Commun.* 1911

[83] Ramirez-Gonzalez P E, Sanchez-Diaz L E, Medina-Noyola M and Wang Y 2016 Communication: Probing the existence of partially arrested states in ionic liquids *J. Chem. Phys.* **145** 191101

[84] Cao W, Wang Y and Saielli G 2018 Metastable state during melting and solid-solid phase transition of [CnMim][NO_3] (n = 4-12) Ionic Liquids by molecular dynamics simulation *J. Phys. Chem.* B **122** 229

[85] Shi R and Wang Y 2016 Dual Ionic and organic nature of ionic liquids *Sci. Rep.* **6** 19644

[86] Weingärtner H 2008 Understanding ionic liquids at the molecular level: facts, problems, and controversies *Angew. Chem. Int. Ed.* **47** 654

[87] Chandler D, Weeks J D and Andersen H C 1983 Van der Waals picture of liquids, solids, and phase transformations *Science* **220** 787

[88] Del Pópolo M G and Voth G A 2004 On the structure and dynamics of ionic liquids *J. Phys. Chem.* B **108** 1744

[89] Hu Z and Margulis C J 2006 Heterogeneity in a room-temperature ionic liquid: persistent local environments and the red-edge effect *Proc. Natl Acad. Sci.* **103** 831

[90] Huang X, Margulis C J, Li Y and Berne B J 2005 Why is the partial molar volume of CO_2 so small when dissolved in a room temperature ionic liquid? Structure and dynamics of CO_2 dissolved in [Bmim+][PF6-] *J. Am. Chem. Soc.* **127** 17842

[91] Karimi-Varzaneh H A, Müller-Plathe F, Balasubramanian S and Carbone P 2010 Studying long-time dynamics of imidazolium-based ionic liquids with a systematically coarse-grained model *Phys. Chem. Chem. Phys.* **12** 4714

[92] Kohagen M, Brehm M, Thar J, Zhao W, Müller-Plathe F and Kirchner B 2011 Performance of quantum chemically derived charges and persistence of ion cages in ionic liquids. A molecular dynamics simulations study of 1-n-butyl-3-methylimidazolium bromide *J. Phys. Chem.* B **115** 693

[93] Morrow T I and Maginn E J 2002 Molecular dynamics study of the ionic liquid 1-n-butyl-3-methylimidazolium hexafluorophosphate *J. Phys. Chem.* B **106** 12807

[94] Shi R and Wang Y 2013 Ion-cage interpretation for the structural and dynamic changes of ionic liquids under an external electric field *J. Phys. Chem.* B **117** 5102

[95] Zahn S, Thar J and Kirchner B 2010 Structure and dynamics of the protic ionic liquid monomethylammonium nitrate ($[CH_3\ NH_3][NO_3]$) from ab initio molecular dynamics simulations *J. Chem. Phys.* **132** 124506

[96] Zhang Y and Maginn E J 2015 Direct correlation between ionic liquid transport properties and ion pair lifetimes: A molecular dynamics study *J. Phys. Chem. Lett.* **6** 700

[97] Lynden-Bell R, Hutchinson D and Doyle M 1986 Translational molecular motion and cages in computer molecular liquids *Mol. Phys.* **58** 307

[98] Lynden-Bell R and Steele W A 1984 A model for strongly hindered molecular reorientation in liquids *J. Phys. Chem.* **88** 6514

[99] Polissar M J 1938 A Kinetic approach to the theory of conductance of infinitely dilute solutions, based on the``Cage'model of liquids *J. Chem. Phys.* **6** 833

[100] Rabani E, Gezelter J D and Berne B 1997 Calculating the hopping rate for self-diffusion on rough potential energy surfaces: Cage correlations *J. Chem. Phys.* **107** 6867

[101] Turton D A, Hunger J, Stoppa A, Thoman A, Candelaresi M, Hefter G, Walther M, Buchner R and Wynne K 2011 Rattling the cage: micro-to mesoscopic structure in liquids as simple as argon and as complicated as water *J. Mol. Liq.* **159** 2

[102] Fujisawa T, Nishikawa K and Shirota H 2009 Comparison of interionic/intermolecular vibrational dynamics between ionic liquids and concentrated electrolyte solutions *J. Chem. Phys.* **131** 244519

[103] Triolo A, Russina O, Bleif H-J and Di Cola E 2007 Nanoscale segregation in room temperature ionic liquids *J. Phys. Chem.* B **111** 4641

[104] Wang Y, Jiang W, Yan T and Voth G A 2007 Understanding ionic liquids through atomistic and coarse-grained molecular dynamics simulations *Acc. Chem. Res.* **40** 1193

[105] Raju S and Balasubramanian S 2010 Role of cation symmetry in intermolecular structure and dynamics of room temperature ionic liquids: simulation studies *J. Phys. Chem.* B **114** 6455

[106] Xiao D, Hines L G Jr, Li S, Bartsch R A, Quitevis E L, Russina O and Triolo A 2009 Effect of cation symmetry and alkyl chain length on the structure and intermolecular dynamics of 1, 3-dialkylimidazolium bis (trifluoromethanesulfonyl) amide ionic liquids *J. Phys. Chem.* B **113** 6426

[107] Canongia Lopes J N and Pádua A A 2006 Nanostructural organization in ionic liquids *J. Phys. Chem.* B **110** 3330

[108] Canongia Lopes J N, Costa Gomes M F and Pádua A A 2006 Nonpolar, polar, and associating solutes in ionic liquids *J. Phys. Chem.* B **110** 16816

[109] Santos L M, Canongia Lopes J N, Coutinho J A, Esperança J M, Gomes L R, Marrucho I M and Rebelo L P 2007 Ionic liquids: first direct determination of their cohesive energy *J. Am. Chem. Soc.* **129** 284

[110] Axenov K V and Laschat S 2011 Thermotropic ionic liquid crystals *Materials* **4** 206

[111] Goossens K, Lava K, Nockemann P, Van Hecke K, Van Meervelt L, Driesen K, Görller-Walrand C, Binnemans K and Cardinaels T 2009 Pyrrolidinium ionic liquid crystals *Chem. Euro. J.* **15** 656

[112] Guillet E, Imbert D, Scopelliti R and Bünzli J-C G 2004 Tuning the emission color of europium-containing ionic liquid-crystalline phases *Chem. Mater.* **16** 4063

[113] Kouwer P H and Swager T M 2007 Synthesis and mesomorphic properties of rigid-core ionic liquid crystals *J. Am. Chem. Soc.* **129** 14042

[114] Starkulla G F, Klenk S, Butschies M, Tussetschläger S and Laschat S 2012 Towards room temperature ionic liquid crystals: linear versus bent imidazolium phenylpyrimidines *J. Mater. Chem.* **22** 21987

[115] Causin V and Saielli G 2009 Effect of asymmetric substitution on the mesomorphic behaviour of low-melting viologen salts of bis (trifluoromethanesulfonyl) amide *J. Mater. Chem.* **19** 9153

[116] Li S and Wang Y 2019 Percolation phase transition from ionic liquids to ionic liquid crystals *Sci. Rep.* **9** 13169

[117] Sahimi M 1994 (Book) Sahimi, M., Applications of Percolation Theory. Taylor & Francis Ltd: London, 1994. *Applications of Percolation Theory* (London: Taylor & Francis Ltd) p 20

[118] Stauffer D and Aharony A 1992 (Book) Stauffer, D.; Aharony, A., Introduction to Percolation Theory. Taylor & Francis: London, 1992. *Introduction to Percolation Theory* (London: Taylor & Francis) p 15

[119] Saielli G, Bagno A and Wang Y 2015 Insights on the isotropic-to-smectic A transition in ionic liquid crystals from coarse-grained molecular dynamics simulations: the role of microphase segregation *J. Phys. Chem.* B **119** 3829

[120] Saielli G and Wang Y 2016 Role of the electrostatic Interactions in the Stabilization of ionic liquid crystals: insights from coarse-grained MD simulations of an imidazolium model *J. Phys. Chem.* B **120** 9152

[121] Bowlas C J, Bruce D W and Seddon K R 1996 Liquid-crystalline ionic liquids *Chem. Commun.* 1625

[122] Abe H and Kishimura H 2022 Multistep phase transition in 1-decyl-3-methylimidazolium nitrate ionic liquid *J. Mol. Liq.* **352** 118695

[123] Sanchez-Diaz L E, Vizcarra-Rendon A and Juarez-Maldonado R 2009 Ionic and Wigner glasses, superionic conductors, and spinodal electrostatic gels: dynamically arrested phases of the primitive model *Phys. Rev. Lett.* **103** 035701

[124] Juárez-Maldonado R and Medina-Noyola M 2008 Theory of dynamic arrest in colloidal mixtures *Phys. Rev.* E **77** 051503

[125] Blesic M, Lopes J N C, Padua A A, Shimizu K, Gomes M F C and Rebelo L P N 2009 Phase equilibria in ionic liquid− aromatic compound mixtures, including benzene fluorination effects *J. Phys. Chem.* B **113** 7631

[126] Deetlefs M, Hardacre C, Nieuwenhuyzen M, Sheppard O and Soper A K 2005 Structure of ionic liquid− benzene mixtures *J. Phys. Chem.* B **109** 1593

[127] Gonfa G, Bustam M A, Muhammad N and Ullah S 2017 Effect of task specific thiocyanate based ionic liquids on relative volatility of cyclohexane and benzene azeotropic mixture *J. Mol. Liq.* **238** 208

[128] Holbrey J D, Reichert W M, Nieuwenhuyzen M, Sheppard O, Hardacre C and Rogers R D 2003 Liquid clathrate formation in ionic liquid–aromatic mixtures *Chem. Commun.* 476

[129] Łachwa J, Bento I, Duarte M T, Lopes J N C and Rebelo L P 2006 Condensed phase behaviour of ionic liquid–benzene mixtures: congruent melting of a $[emim][NTf_2]\cdot C_6H_6$ inclusion crystal *Chem. Commun.* 2445

[130] Lee E C, Kim D, Jurecka P, Tarakeshwar P, Hobza P and Kim K S 2007 Understanding of assembly phenomena by aromatic− aromatic interactions: benzene dimer and the substituted systems *J. Phys. Chem.* A **111** 3446

[131] Pereira J F, Flores L A, Wang H and Rogers R D 2014 Benzene solubility in ionic liquids: working toward an understanding of liquid clathrate formation *Chem. Euro. J.* **20** 15482

[132] Shimomura T, Takamuku T and Yamaguchi T 2011 Clusters of imidazolium-based ionic liquid in benzene solutions *J. Phys. Chem.* B **115** 8518
[133] Shirota H, Kakinuma S, Itoyama Y, Umecky T and Takamuku T 2016 Effects of tetrafluoroborate and bis (trifluoromethylsulfonyl) amide anions on the microscopic structures of 1-methyl-3-octylimidazolium-based ionic liquids and benzene mixtures: a multiple approach by ATR-IR, NMR, and Femtosecond Raman-induced Kerr effect spectroscopy *J. Phys. Chem.* B **120** 513
[134] Li S, Saielli G and Wang Y 2018 Aggregation behavior of dihexadecylviologen bistriflimide ionic liquid crystal in different solvents: influence of polarity and concentration *Phys. Chem. Chem. Phys.* **20** 22730
[135] Li S, Safari N, Saielli G and Wang Y 2020 Liquid-liquid phase separation of viologen bistriflimide/benzene mixtures: role of the dual ionic and organic nature of ionic liquids *J. Phys. Chem.* B **124** 7929
[136] Bystrov S S, Matveev V V, Egorov A V, Chernyshev Y S, Konovalov V A, Balevičius V and Chizhik V I 2019 Translational diffusion in a set of imidazolium-based ionic liquids [bmim]+ A–and their mixtures with water *J. Phys. Chem.* B **123** 9187
[137] Carrete J, Mendez-Morales T, Cabeza O, Lynden-Bell R M, Gallego L J and Varela L M 2012 Investigation of the local structure of mixtures of an ionic liquid with polar molecular species through molecular dynamics: Cluster formation and angular distributions *J. Phys. Chem.* B **116** 5941
[138] D'Angelo P, Zitolo A, Aquilanti G and Migliorati V 2013 Using a combined theoretical and experimental approach to understand the structure and dynamics of imidazolium-based ionic liquids/water mixtures. 2. EXAFS spectroscopy *J. Phys. Chem.* B **117** 12516
[139] Ghatee M H and Zolghadr A R 2013 Local depolarization in hydrophobic and hydrophilic ionic liquids/water mixtures: car–parrinello and classical molecular dynamics simulation *J. Phys. Chem.* C **117** 2066
[140] Hegde G A, Bharadwaj V S, Kinsinger C L, Schutt T C, Pisierra N R and Maupin C M 2016 Impact of water dilution and cation tail length on ionic liquid characteristics: Interplay between polar and non-polar interactions *J. Chem. Phys.* **145** 064504
[141] Koishi T 2018 Molecular dynamics study of the effect of water on hydrophilic and hydrophobic ionic liquids *J. Phys. Chem.* B **122** 12342
[142] Migliorati V, Zitolo A and D'Angelo P 2013 Using a combined theoretical and experimental approach to understand the structure and dynamics of imidazolium-based ionic liquids/water mixtures. 1. MD simulations *J. Phys. Chem.* B **117** 12505
[143] Moreno M, Castiglione F, Mele A, Pasqui C and Raos G 2008 Interaction of water with the model ionic liquid [bmim] $[BF_4]$: molecular dynamics simulations and comparison with NMR data *J. Phys. Chem.* B **112** 7826
[144] Nickerson S D, Nofen E M, Chen H, Ngan M, Shindel B, Yu H and Dai L L 2015 A combined experimental and molecular dynamics study of iodide-based ionic liquid and water mixtures *J. Phys. Chem.* B **119** 8764
[145] Schröder C, Rudas T, Neumayr G, Benkner S and Steinhauser O 2007 On the collective network of ionic liquid/water mixtures. I. Orientational structure *J. Chem. Phys.* **127** 234503
[146] Vicent-Luna J M, Dubbeldam D, Gómez-Álvarez P and Calero S 2016 Aqueous solutions of ionic liquids: microscopic assembly *ChemPhysChem* **17** 380
[147] Jiang W, Wang Y and Voth G A 2007 Molecular dynamics simulation of nanostructural organization in ionic liquid/water mixtures *J. Phys. Chem.* B **111** 4812
[148] Ohta S, Shimizu A, Abe H, Hatano N, Ima Y and Yoshimura Y 2011 Peculiar concentration dependence of H/D exchange reaction in 1-butyl-3-methylimidazolium tetrafluoroborate-D_2O mixtures *Open J. Phys. Chem.* **1** 70
[149] Abe H, Takekiyo T, Shigemi M, Yoshimura Y, Tsuge S, Hanasaki T, Ohishi K, Takata S and Suzuki J-I 2014 Direct evidence of confined water in room-temperature ionic liquids by complementary use of small-angle X-ray and neutron scattering *J. Phys. Chem. Lett.* **5** 1175
[150] Abe H, Takekiyo T, Yoshimura Y, Saihara K and Shimizu A 2016 Anomalous freezing of nano-confined water in room-temperature ionic liquid 1-butyl-3-methylimidazolium nitrate *ChemPhysChem* **17** 1136
[151] Saihara K, Yoshimura Y, Ohta S and Shimizu A 2015 Properties of water confined in ionic liquids *Sci. Rep.* **5** 1
[152] Bernardes C E, Minas da Piedade M E and Canongia Lopes J N 2011 The structure of aqueous solutions of a hydrophilic ionic liquid: the full concentration range of 1-ethyl-3-methylimidazolium ethylsulfate and water *J. Phys. Chem.* B **115** 2067
[153] Hayes R, Warr G G and Atkin R 2015 Structure and nanostructure in ionic liquids *Chem. Rev.* **115** 6357
[154] Shimizu K, Bernardes C E and Canongia Lopes J N 2014 Structure and aggregation in the 1-alkyl-3-methylimidazolium bis (trifluoromethylsulfonyl) imide ionic liquid homologous series *J. Phys. Chem.* B **118** 567
[155] Shimizu K, Gomes M F C, Pádua A A, Rebelo L P and Lopes J N C 2010 Three commentaries on the nano-segregated structure of ionic liquids *J. Mol. Struct. Theochem.* **946** 70
[156] Russina O, Lo Celso F, Plechkova N V and Triolo A 2017 Emerging evidences of mesoscopic-scale complexity in neat ionic liquids and their mixtures *J. Phys. Chem. Lett.* **8** 1197
[157] Cosby T, Kapoor U, Shah J K and Sangoro J 2019 Mesoscale Organization and Dynamics in Binary Ionic Liquid Mixtures *J. Phys. Chem. Lett.* **10** 6274
[158] Fuladi S, Gholivand H, Ahmadiparidari A, Curtiss L A, Salehi-Khojin A and Khalili-Araghi F 2021 Multicomponent Phase Separation in Ternary Mixture Ionic Liquid Electrolytes *J. Phys. Chem.* B **125** 7024